

# A First Extension of Geometric Control Theory to Underwater Vehicles<sup>★</sup>

Monique Chyba<sup>\*</sup> Ryan N. Smith<sup>\*\*</sup>

<sup>\*</sup> *Mathematics Department, e-mail: mchyba@math.hawaii.edu*

<sup>\*\*</sup> *Ocean & Resources Engineering Department,  
e-mail: ryan@ore.hawaii.edu*

*University of Hawaii at Manoa, Honolulu, HI 96822 USA*

---

**Abstract:** This paper serves as a first study on the implementation of control strategies developed using a kinematic reduction onto test bed autonomous underwater vehicles (AUVs). The equations of motion are presented in the framework of differential geometry, including external dissipative forces, as a forced affine connection control system. We show that the hydrodynamic drag forces can be included in the affine connection, resulting in an affine connection control system. The definitions of kinematic reduction and decoupling vector field are thus extended from the ideal fluid scenario. Control strategies are computed using this new extension and are reformulated for implementation onto a test-bed AUV. We compare these geometrically computed controls to time and energy optimal controls for the same trajectory which are computed using a previously developed algorithm. Through this comparison we are able to validate our theoretical results based on the experiments conducted using the time and energy efficient strategies.

Keywords: Autonomous Underwater Vehicles, Kinematic Reduction, Under-actuated, Decoupling Vector Field, Dissipative, Potential Force

---

## 1. INTRODUCTION

Autonomous Underwater Vehicles (AUVs) have proven to be an asset in many areas of oceanographic research. With this ever increasing role, research has turned its focus to examine the control of such vehicles. In this paper, we address this research interest via the implementation of control strategies developed using a differential geometric approach. This architecture allows us to exploit the inherent nonlinear dynamic structure of AUVs and other mechanical systems.

To begin, we present the equations of motion for a rigid body submerged in a real fluid subject to external potential and dissipative forces. We write these equations as a forced affine connection control system (FACCS) on the differentiable configuration manifold,  $Q = \mathbb{R}^3 \times \text{SO}(3) = \text{SE}(3)$ . See Bullo and Lewis (2005) for a treatise on affine connection control systems.

Without these external forces (considering the body in an ideal fluid), we can express the equations of motion as an affine connection control system. For a general affine connection control system, Bullo and Lewis (2005) and Bullo and Lynch (2001) have defined the notions of a kinematic reduction and decoupling vector field. In the ideal fluid case, we can use these notions to compute some solutions to the motion planning problem for AUVs. Unfortunately, these solutions can not be implemented on a test-bed vehicle because the neglected external forces

play a major role in the dynamics of the vehicle. Currently, a characterization of a kinematic reduction for the FACCS which includes the external dissipative and potential forces experienced by a real vehicle does not exist. Hence, we must look to extend the known theory in order to compute solutions to the motion planning problem which can be implemented onto a real AUV.

We are motivated to extend geometric control theory because of its ability to provide solutions to the motion planning problem for an under-actuated system. In practice, AUVs can, and often do, have actuator failure. Implementing a control strategy that can account for such failures provides a higher probability of recovering a damaged vessel.

Here we focus on the construction of a first extension to the characterization of the kinematic reduction to the FACCS. For this initial step, we assume that the vehicle is neutrally buoyant and that the center of gravity ( $C_G$ ) and center of buoyancy ( $C_B$ ) coincide. These assumptions directly imply the omission of the potential forces of buoyancy and gravity. For this first step, we strictly focus only on the dissipative forces. The dissipative forces arise due to fluid shear stresses and are commonly referred to as hydrodynamic drag forces. In Catone et al. (2008), we demonstrate how such forces can be included into the affine connection, thus allowing us to extend the characterization of kinematic reduction and decoupling vector field to include some external forces.

With this new extension, we construct control strategies for a given initial and final configuration of the vehicle.

---

<sup>★</sup> Research funded in part by NSF grant DMS-0608583. Travel funded in part by the Graduate Student Organization of the University of Hawaii at Manoa.

These strategies are then compared to previously implemented strategies for which the initial and final configurations are the same. These previously implemented strategies were numerically computed using algorithms developed to examine the time and energy consumption optimal motion planning problem for AUVs. In the numerically computed strategies, the full dynamic model is integrated and thus potential forces are fully accounted for. In both cases, theoretical predictions compared excellently with experimental results, see Chyba et al. (2008b) and Chyba et al. (2007) for examples. Thus, comparing our geometrically constructed control strategies with those which we have already tested and validated in previous research, will provide information on the accuracy and validity of the underlying theory.

To further validate the theory we are planning to implement the geometrically derived control strategies onto a test-bed AUV. This paper is the first step towards practical applications of geometric control theory on AUVs. The implementation of our motions will also demonstrate the need for the inclusion of potential forces in the theory. Experiments are planned and research is currently active in this area.

## 2. EQUATIONS OF MOTION

Here we state the general equations of motion for an AUV in a real fluid. For a detailed derivation of these equations along with physical explanations for each of the terms, please see Bullo and Lewis (2005) or Catone et al. (2008).

*Fact 1.* The equations of motion for a general simple mechanical control system (rigid body) submerged in a real fluid subjected to external forces can be written as

$$\begin{aligned} \nabla_{\gamma'} \gamma' &= -\text{grad } V_G(\gamma(t)) - \text{grad } V_B(\gamma(t)) \\ &+ \mathbb{G}^\#(F(\gamma'(t))) + \sum_{i=1}^6 \mathbb{I}_i^{-1}(\gamma(t)) \sigma_i(t), \end{aligned} \quad (1)$$

where  $\text{grad } V_G(\gamma(t))$  represents the potential force from gravity and  $\text{grad } V_B(\gamma(t))$  represents the potential force from the vehicle's buoyancy,  $\mathbb{G}^\#(F(\gamma'(t)))$  represents the dissipative drag force,  $\mathbb{I}_i^{-1} = \mathbb{G}^\# \pi_i = \mathbb{G}^{ij} X_j$ , which may be represented as the  $i^{\text{th}}$  column of the matrix  $\mathbb{I}^{-1} = \begin{pmatrix} M^{-1} & 0 \\ 0 & J^{-1} \end{pmatrix}$ , and  $\sigma_i(t)$  are the controls. The  $M$  and  $J$  are  $3 \times 3$  matrices which account for the mass and added mass of the vehicle. These matrices are diagonal since our test-bed vehicle has three planes of symmetry and the origin of the body-fixed reference frame is located at  $(C_G)$ .

### 2.1 Simplified Equations of Motion

For the rest of the paper, we make some assumptions which simplify these equations slightly. We assume that the rigid body is neutrally buoyant and that  $C_G = (C_B)$ ; this eliminates the external potential forces  $V_G(\gamma(t))$  and  $V_B(\gamma(t))$ . Practically speaking, the neutrally buoyant assumption is not very restrictive since most vehicles are near neutral and have the means to make themselves neutral either by taking on ballast or applying a force with it's actuators. On the other hand, the assumption  $C_G = C_B$  is not very practical. This puts the vehicle in a condition of neutral stability, which is not how underwater

vehicles are generally designed. Under these assumptions, we rewrite (1) as

$$\nabla_{\gamma'} \gamma' = \mathbb{G}^\#(F(\gamma'(t))) + \sum_{i=1}^6 \mathbb{I}_i^{-1}(\gamma(t)) \sigma_i(t), \quad (2)$$

## 3. THE MODIFIED CONNECTION

In (2) we have a FACCS which is represented by an affine connection control system along with an additional external vector field. Current theory utilizing kinematic reductions does not support such systems. Thus, we show how to include the viscous drag in the affine connection in order to culminate with an affine connection on which to apply known theory.

The magnitude of the drag force acting on a rigid body is proportional to the square of the velocity of the body (i.e.  $D = C_D \rho A \nu |\nu|$ ). Since a vehicle may have different drag coefficients and different projected areas depending on the direction of the velocity, we define  $D_i = C_{D_i} \rho A_i$  where  $i \in \{1, \dots, 6\}$  denotes the respective degree of freedom in which the velocity is applied. Then we let  $\mathcal{D}_i = \frac{D_i}{m_i} \nu_i^2$  for  $i = 1, 2, 3$  and  $\mathcal{D}_i = \frac{D_i}{j_{i-3}} \Omega_{i-3}^2$  for  $i = 4, 5, 6$ . For this study, we determine the trajectory and compute the associated control structure along that path. Thus, we know the direction of motion and can conscientiously eliminate the absolute value in the first relation. Now, the drag force depends only on the square of the velocity of the body along a given trajectory  $\gamma$ . Given that the standard basis for  $\text{SE}(3)$  is  $\{X_1, \dots, X_6\}$  with dual basis  $\{\pi^1, \dots, \pi^6\}$ , we can write  $F_{drag}(\gamma'(t)) = \sum_1^3 F_i(\gamma'(t)) \nu_i^2 \pi^i + \sum_{i=4}^6 F_{i+3}(\gamma'(t)) \Omega_{i-3}^2 \pi^i$ . Thus, we have the following expression

$$\begin{aligned} &\mathbb{G}^\#(F_{drag}(\gamma'(t))) \\ &= \sum_{i=1}^3 \frac{F_i(\gamma'(t))}{\mathbb{G}_{ii}} \nu_i^2 X_i + \sum_{i=4}^6 \frac{F_i(\gamma'(t))}{\mathbb{G}_{ii}} \Omega_{i-3}^2 X_i \\ &= \sum_{i=1}^6 \mathcal{D}_i X_i, \end{aligned} \quad (3)$$

where  $\mathbb{G}_{ij}$  is the  $i, j$ -entry of the kinetic energy matrix. This relationship allows us to describe the geometric acceleration associated to the viscous drag forces as a symmetric type (1,2)-tensor field on  $\text{SE}(3)$ . Since the difference between any two affine connections is a type (1,2)-tensor field  $\Delta$ , we can incorporate viscous drag into a new connection  $\tilde{\nabla}$  by

$$\tilde{\nabla}_X Y = \nabla_X Y + \Delta(X, Y). \quad (4)$$

In general, a symmetric type (1,2)-tensor is given by

$$\Delta = \sum_{i,j,k} \Delta_{jk}^i X_i \otimes \pi^j \otimes \pi^k, \quad (5)$$

where  $\Delta_k^i j = \Delta_j^i k$ . Computing the above, we get

$$\Delta(X_i, X_j) = \Delta_{ij}^1 X_1 + \dots + \Delta_{ij}^6 X_6. \quad (6)$$

Using equation (3), we have that  $\Delta(X_i, X_i) = \Delta_{ii}^i X_i = \frac{\mathcal{D}_i}{\mathbb{G}_{ii}} X_i$ . Thus, we are able to define the new connection in the following way

$$\tilde{\nabla}_{X_i} X_j = \begin{cases} \frac{\mathcal{D}_i}{\mathbb{G}_{ii}} X_i & i = j \\ \nabla_{X_i} X_j & i \neq j \end{cases}, \quad (7)$$

Table 1. Covariant derivatives in basis notation for the connection  $\tilde{\nabla}$ . We use  $(i, j) = \nabla_{\mathbb{I}_i^{-1}} \mathbb{I}_j^{-1}$ .

(1, 1)	$\frac{D_1}{m_1} X_1$	(2, 1)	$-\frac{1}{2} \frac{(m_1 - m_2)}{j_3} X_6$
(1, 2)	$-\frac{1}{2} \frac{(m_1 - m_2)}{j_3} X_6$	(2, 2)	$\frac{D_2}{m_2} X_2$
(1, 3)	$-\frac{1}{2} \frac{(m_3 - m_1)}{j_2} X_5$	(2, 3)	$\frac{1}{2} \frac{(m_3 - m_2)}{j_1} X_4$
(1, 4)	0	(2, 4)	$-\frac{1}{2} \frac{(m_3 - m_2)}{m_3} X_3$
(1, 5)	$\frac{1}{2} \frac{(m_3 - m_1)}{m_3} X_3$	(2, 5)	0
(1, 6)	$\frac{1}{2} \frac{(m_1 - m_2)}{m_2} X_2$	(2, 6)	$\frac{1}{2} \frac{(m_1 - m_2)}{m_1} X_1$
(3, 1)	$-\frac{1}{2} \frac{(m_3 - m_1)}{j_2} X_5$	(4, 1)	0
(3, 2)	$\frac{1}{2} \frac{(m_3 - m_2)}{j_1} X_4$	(4, 2)	$\frac{1}{2} \frac{(m_3 + m_2)}{m_3} X_3$
(3, 3)	$\frac{D_3}{m_3} X_3$	(4, 3)	$-\frac{1}{2} \frac{(m_3 + m_2)}{m_2} X_2$
(3, 4)	$-\frac{1}{2} \frac{(m_3 - m_2)}{m_2} X_2$	(4, 4)	$\frac{D_4}{j_1} X_4$
(3, 5)	$\frac{1}{2} \frac{(m_3 - m_1)}{m_1} X_1$	(4, 5)	$\frac{1}{2} \frac{(j_3 + j_2 - j_1)}{j_3} X_6$
(3, 6)	0	(4, 6)	$-\frac{1}{2} \frac{(j_3 + j_2 - j_1)}{j_2} X_5$
(5, 1)	$-\frac{1}{2} \frac{(m_3 + m_1)}{m_3} X_3$	(6, 1)	$\frac{1}{2} \frac{(m_2 + m_1)}{m_2} X_2$
(5, 2)	0	(6, 2)	$-\frac{1}{2} \frac{(m_2 + m_1)}{m_1} X_1$
(5, 3)	$\frac{1}{2} \frac{(m_3 + m_1)}{m_1} X_1$	(6, 3)	0
(5, 4)	$-\frac{1}{2} \frac{(j_3 - j_2 + j_1)}{j_3} X_6$	(6, 4)	$-\frac{1}{2} \frac{(j_3 - j_2 - j_1)}{j_2} X_5$
(5, 5)	$\frac{D_5}{j_2} X_5$	(6, 5)	$\frac{1}{2} \frac{(j_3 - j_2 - j_1)}{j_1} X_4$
(5, 6)	$\frac{1}{2} \frac{(j_3 - j_2 + j_1)}{j_1} X_4$	(6, 6)	$\frac{D_6}{j_3} X_6$

since we know  $\nabla_{X_i} X_i = 0$  (see Catone et al. (2008) for more details on this construction).

With this new connection, the equations of motion for the forced affine connection control system become

$$\tilde{\nabla}_{\gamma'} \gamma' = \sum_{a=1}^6 \sigma^a(t) \mathbb{I}_a^{-1}(\gamma(t)). \quad (8)$$

The above system is a second order affine connection control system (ACCS) on SE(3). At first it looks as though we neglect the drag forces, but they are now captured in the new connection  $\tilde{\nabla}$ .

#### 4. CONTROL STRATEGY

Now that we have expressed (2) as an ACCS, we can apply known techniques to determine the decoupling vector fields. Decoupling vector fields are kinematic reductions of rank one. The integral curves of these vector fields define the admissible motions for kinematic control inputs. We call these integral curves the kinematic motions. By concatenating kinematic motions, we can compute solutions to the motion planning problem.

A necessary and sufficient condition for a vector field  $V$  to be decoupling for an affine connection control system is that  $V$  and  $\nabla_V V$  are sections of the input distribution of vector fields. Thus, decoupling vector fields are calculated by considering the covariant derivatives of the input vector fields to the system. Using the new connection  $\tilde{\nabla}$ , we can compute the covariant derivatives of the input vector fields in basis notation corresponding to motion in a real fluid. Results are displayed in table 1. Before we develop the control strategy from these motions, we must first discuss the AUV hydrodynamic parameters assumed in this study.

Table 2. Estimated drag ( $D_i$ ) and added mass ( $m_i, j_i$ ),  $i = 1, 2, 3$  values.

$D_1$	325	$D_2$	325	$D_3$	325
$D_4$	25	$D_5$	25	$D_6$	20
$m_1$	196	$m_2$	196	$m_3$	196
$j_1$	5.46	$j_2$	5.29	$j_3$	5.72

#### 4.1 Hydrodynamic Parameters

Since we compare our control strategies with those in Chyba et al. (2008a), the computations in this paper are based on their parameters. The vehicle has three planes of symmetry and is controlled using eight independent thrusters. We can decouple the actions of these thrusters such that four of the thrusters ( $T_V$ ) control surge, sway and yaw, while the other four ( $T_H$ ) control roll, pitch and heave. This paper designs strategies which utilize a six dimensional control scheme (6-DOF controls) with controls denoted by  $\{\sigma_1, \dots, \sigma_6\}$ . It is important to understand that these controls do not directly correspond to actuator controls. In the case of implementation purposes, we can compute the controls for the eight thrusters, denoted by  $\{\gamma_1, \dots, \gamma_8\}$ , from the given 6-DOF controls via a transformation matrix. The details of this transformation can be found in Chyba et al. (2008b)

Table 2 displays the parameters used in this paper. The mass and added mass terms are those stated in Chyba et al. (2008b). The values for  $D_i$  are estimated from this reference as well. There, the authors estimate form drag using a cubic polynomial with no quadratic or constant term. Here we approximated this cubic function using a quadratic function over the range of velocities we consider for our kinematic motions. Note that in a different velocity range, the values of the  $D_i$  listed here may not be accurate. In the fully-actuated case, any configuration can be realized through the concatenation of at most six pure motions. To provide strategies for a damaged vehicle as mentioned previously, we consider the under-actuated situation. By under-actuated, we are unable to directly control one or more of the six degrees of freedom. Based on the assumed vehicle, there are two basic under-actuated situations which arise naturally and deserve first consideration. First is the loss of thruster set  $T_H$ . This leaves us only able to directly control heave, roll and pitch. Similarly, the other scenario is the loss of thruster set  $T_V$  which leaves us only having direct control on surge, sway and yaw.

Before we begin to discuss the control strategies, we must make one remark about their structure. Since our end goal is to implement such strategies onto actual vehicles, we must take the physical actuators into account. Three main features to note are a finite limit on the thrust which can be prescribed in each DOF, the incapability of instantaneous switches from one direction to the other, and a continuously evolving control strategy requires too much on-board data storage to be practical. The combination of these three limitations leads us to construct strategies which are piece-wise constant with the pieces connected via linear junctions over a short time duration. This duration depends on the thrusters and the considered vehicle, and should be the shortest span which allows for a

switch from maximum forward thrust to maximum reverse thrust without damaging the thruster.

#### 4.2 Horizontal Thrusters Only

This scenario represents a loss of all four vertical thrusters ( $T_V$ ), and permits direct control only upon surge, sway and yaw. We refer to this as a three input system since the only input control vector fields for the system are  $\mathbb{I}_1^{-1} = (\frac{1}{m_1}, 0, 0, 0, 0, 0)^t$ ,  $\mathbb{I}_2^{-1} = (0, \frac{1}{m_2}, 0, 0, 0, 0)^t$ , and  $\mathbb{I}_6^{-1} = (0, 0, 0, 0, 0, \frac{1}{j_3})^t$ . The decoupling vector fields for this system are the constant multiples and linear combinations of the set  $\mathcal{V} = \{X_1 = (1, 0, 0, 0, 0, 0), X_2 = (0, 1, 0, 0, 0, 0), X_6 = (0, 0, 0, 0, 0, 1)\}$ . We note here that vehicle motions are thus restricted to a plane, see Chyba et al. (2007). Due to the symmetry in the coefficients, the pure surge and pure sway motions are identical. In this under-actuated scenario, it is enough to examine a pure surge motion, as any reachable configuration will be a concatenation of pure surge and pure sway motions with possibly a yaw displacement upon realizing the final translational displacement. We prescribe a pure surge motion of  $5m$ , with final configuration  $\eta_{F_1} = (5, 0, 0, 0, 0, 0)$ . This trajectory will serve two purposes for our study. First, we will be able to assess the estimated drag values for surge (sway) and be able to fine tune our model with respect to the dissipative forces. We will demonstrate the extension of the kinematic reduction by producing a control strategy which incorporates drag forces.

#### 4.3 Pure Surge ( $\eta_{F_1}$ ) Control Strategy

For this motion, we need only consider the decoupling vector field  $X_1$ . We then use Theorem 13.5 in Bullo and Lewis (2005) to compute the associated control structure of  $\sigma^1(t)$  as follows:

$$\sigma^1(t)\mathbb{I}_1^{-1}(\gamma \circ \tau(t)) = (\tau'(t))^2 \nabla_{X_1} X_1(\gamma \circ \tau(t)) + \tau''(t) X_1(\gamma \circ \tau(t)), \quad (9)$$

where  $\tau(t)$  is a reparameterization of the curve  $\gamma(t)$  such that the vehicle will begin and end the motion with zero velocity. Since  $X_1$  is the decoupling vector field,  $\gamma(t) = (t, 0, 0, 0, 0, 0)$  and we choose  $\tau(t) : [0, 30] \mapsto [0, 5]$  to be  $\tau(t) = \frac{t^2(45-t)}{2700}$ . Thus we can compute the control from

$$m_1 \sigma^1(t) = D_1(\tau'(t))^2 + \tau''(t). \quad (10)$$

Substituting, we get that  $\sigma^1(t) = \frac{1}{32400}(13t^4 - 780t^3 + 11700t^2 - 14112t + 211680)$ . From this continuous thrust strategy, we can construct a piece-wise constant thrust strategy by integrating  $\sigma^1(t)$  for  $t \in (0, 25.8)$  for the positive acceleration phase and  $t \in (25.8, 30)$  for the deceleration phase. This gives the piece-wise constant control strategy

$$\sigma^1(t) = \begin{cases} 13.2 & t \in [0, 25.8] \\ -3.9 & t \in [25.8, 30] \end{cases}. \quad (11)$$

This strategy matches very well to those which have already been experimentally verified. In particular, if the test-bed AUV is responsible for maintaining a constant depth using a closed-loop feedback control, then the piece-wise constant-time optimal control strategy for a  $5m$  pure surge, given that the maximum and minimum available

forces are  $13N$  and  $-5N$  respectively, is given by the following:

$$\sigma^1(t) = \begin{cases} 13.5 & t \in [0, 24.3] \\ -5 & t \in [24.3, 29.5] \end{cases}. \quad (12)$$

This excellent comparison validates the theoretic model and the inclusion of drag forces into the model for the geometrically generated control strategies. The small discrepancy between these two strategies may be eliminated by using a different reparameterization or modifying  $D_1$ , both of which can only be properly corrected after analyzing implementations results onto a test-bed AUV.

We remark that using a piece-wise constant control strategy as opposed to the computed continuous strategy, alters the velocity profile along the trajectory, however the vehicle will still start and end at zero velocity. This ensures we are able to concatenate multiple kinematic motions to create the desired motion. Since this trajectory is a single motion and not a concatenation, it agrees well with the time optimal trajectory. In the sequel, it is seen that our concatenation of kinematic motions is far from time optimal. In fact, since the vehicle must go through zero velocity states, the concatenation of kinematic motions will never be time optimal.

#### 4.4 Vertical Thrusters Only

This scenario represents a loss of all four horizontal thrusters ( $T_V$ ), and permits direct control only upon roll, pitch and heave. As opposed to the previous condition, this under-actuated scenario is fully kinematically controllable; any configuration is reachable from any other via kinematic motions. This fact is proved in Chyba et al. (2007). The decoupling vector fields for this system are the constant multiples and linear combinations of the set  $\mathcal{V} = \{X_3 = (0, 0, 1, 0, 0, 0), X_4 = (0, 0, 0, 1, 0, 0), X_5 = (0, 0, 0, 0, 1, 0)\}$ . We will examine a trajectory with final configuration given by  $\eta_{F_2} = (5, 4, 1, 0, 0, 0)$ . A similar configuration to  $\eta_{F_2}$  is examined in Chyba et al. (2007) in the case of an ideal fluid.

#### 4.5 Control Strategy for $\eta_{F_2}$

In this scenario, we only have direct control on heave, pitch and roll, however we wish to realize a trajectory that calls for translation in surge, sway and heave. At first it may not be obvious how a vehicle would arrive at  $\eta_{F_2}$  without direct control upon horizontal translation. The basic idea will be to pitch and roll the vehicle to point the body heave axis at the final configuration, then prescribe a body-pure heave to achieve the translation, and then undo the angular displacements. For this trajectory, we will use the decoupling vector field  $W = 1.38X_4 + 1.33X_5$  to realize both the pitch and roll simultaneously, followed by  $V_4$  to realize the heave, and then we will use  $-W$  to undo the pitch and roll.

To construct the control strategy, we choose  $\tau_W(t) : [0, 6] \mapsto [0, 1]$  and  $\tau_{X_3}(t) : [0, 35] \mapsto [0, \sqrt{42}]$ . The choice of the reparameterization time is such that the values of the computed thrusts are within the acceptable range for the thrusters, and the velocity along the trajectory is in the range where our drag estimations hold. Thus, we get

that  $\tau_W(t) = \frac{1}{108}t^2(9-t)$  and  $\tau_{X_3}(t) = \frac{\sqrt{42}}{42875}t^2(105-2t)$ . Following the steps outlined in section 4.3 for each motion, we compute the continuous controls for each integral curve to be

$$\sigma^4(t) = \frac{23}{360000}(575t^4 - 6900t^3 + 20700t^2 - 6552t + 19656), \quad t \in [0, 6], \quad (13)$$

$$\sigma^5(t) = \frac{133}{12960000}(3325t^4 - 39900t^3 + 119700t^2 - 38088t + 114264), \quad t \in [0, 6], \quad (14)$$

$$\sigma^3(t) = \frac{2808t^4}{10504375} - \frac{5616t^3}{300125} + \frac{2808t^2}{8575} - \frac{48\sqrt{42}t}{875} + \frac{24\sqrt{42}t}{25}, \quad t \in [0, 35]. \quad (15)$$

Concatenating the computed controls requires shifting these controls so that they operate at the prescribed time during the trajectory. Computing the piece-wise constant control for each  $\sigma^i(t)$  and then concatenating them together to realize the entire motion gives

$$\sigma(t) = \begin{cases} (0, 0, 0, 2.05, 1.9, 0)^t & t \in [0, 5] \\ (0, 0, 0, -0.7, -0.66, 0)^t & t \in [5, 6] \\ (0, 0, 15.8, 0, 0, 0)^t & t \in [6, 36.7] \\ (0, 0, -3.8, 0, 0, 0)^t & t \in [36.7, 41] \\ (0, 0, 0, -2.05, -1.9, 0)^t & t \in [41, 46] \\ (0, 0, 0, 0.7, 0.66, 0)^t & t \in [46, 47] \end{cases} \cdot (16)$$

## 5. SIMULATIONS

Here we compare the geometrically computed control strategy we designed to terminate at  $\eta_{F_2}$  to those computed in Chyba et al. (2008a). Note that even though the final configurations may be the same, the evolution of the vehicle may differ between the geometric construction and the numerical solution. This discrepancy is due to the optimization algorithm having all the thrusters available to realize the motion (fully-actuated case), while here we consider the under-actuated scenario and do not have direct control on three degrees of freedom. The numerical algorithm used to compute time and energy consumption efficient control strategies is described in detail in Chyba et al. (2008b); we refer to this as the Switching Time Parameterization (STP) algorithm.

### 5.1 Trajectory Duration

In section 4.5, we presented a control strategy connecting the origin to  $\eta_{final} = (5, 4, 1, 0, 0, 0)$  lasting 47 seconds. This strategy is displayed graphically in Fig. 1 and gives the nonzero eight dimensional controls supplied to each thruster over the duration of the motion. The optimal time to realize this displacement is 23.5 seconds, as shown in Chyba et al. (2008c) when considering the 6-DOF controls. In Chyba et al. (2008a), the minimum time is quoted as 17.43 seconds, but is computed using the eight dimensional control domain. The differences between these two can be studied in more detail in Chyba et al. (2008a). For the kinematic motion strategy, computations are made based on the 6-DOF control, yet for comparison, we display the control supplied to each of the eight individual thrusters.

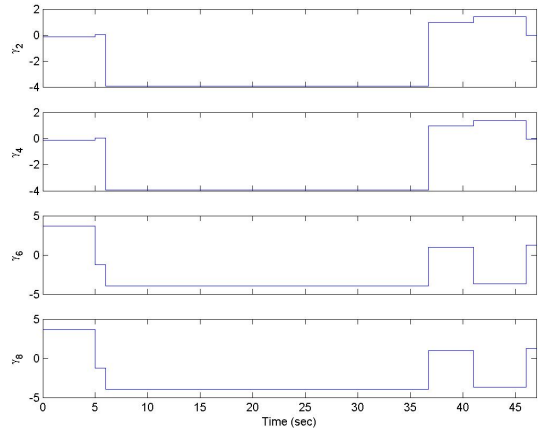


Fig. 1. Individual control supplied to each thruster of  $T_V$  for the kinematic motion ending at  $\eta_{F_2} = (5, 4, 1, 0, 0, 0)$ .

As mentioned previously, the geometrically computed control strategies which involve concatenation can not be time optimal since the trajectory contains periods of zero velocity. However, as mentioned in Chyba et al. (2008b), time optimal trajectories are not implementable onto AUVs due to their complex structure, so the authors present the time efficient  $STP_2$  strategy as an implementable alternative. This strategy has a duration of 25.3 seconds. In Fig. 2 we display the  $STP_2$  control strategy for the same initial and final configurations considered in section 4.5. When

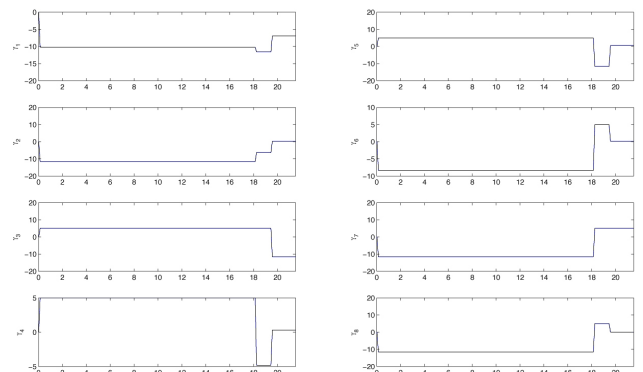


Fig. 2.  $STP_2$  eight dimensional thrust strategy for the time efficient motion ending at  $\eta_{F_2} = (5, 4, 1, 0, 0, 0)$ .

comparing Fig. 1 to Fig. 2, the first thing to note is that the actual motion of the vehicle is quite similar. The  $STP_2$  strategy also points the bottom of the vehicle towards  $\eta_{F_2}$  and utilizes a body-heave to reach its destination. A noticeable difference is the use of the surge and sway DOF to help realize the motion. Since this trajectory was designed to be time efficient, we would expect that all thrusters and DOFs are utilized to some extent. Also, the vehicle does not need to waste thrust maintaining large pitch and roll angles (counteracting potential forces) since additional control in surge and sway is available. This brings us to the next discrepancy, which is in the pitch and roll control. Note that in Fig. 2, the pitch and roll controls are utilized throughout the trajectory. This is to compensate for the righting moment. In the geometric control strategy, we neglect potential forces, thus we do not account for the righting moment. Buoyancy is the other potential force

which is unaccounted for in our control strategy and this can be seen in the slightly higher force applied in heave for the  $STP_2$  strategy.

## 5.2 Energy Consumption

Another aspect of the control strategy computed in section 4.5 which we can examine is the amount of energy consumed during a prescribed motion. In Chyba et al. (2008a), the authors consider the implementation of trajectories which minimize energy consumption. These strategies are derived from an application of the STP algorithm to the consumption minimization problem, since consumption optimal strategies are also not implementable. Strategies derived for this criterion will be denoted  $STP^E$ . The consumption criterion is based on the consumption of the thrusters, and details can be found in the cited reference. For the set of initial and final configurations we examine here, the implementable  $STP_2^E$  control strategy has a consumption of 163.89Ah and a duration of 35 seconds. We display the control structure in Fig. 3. Here, we see that

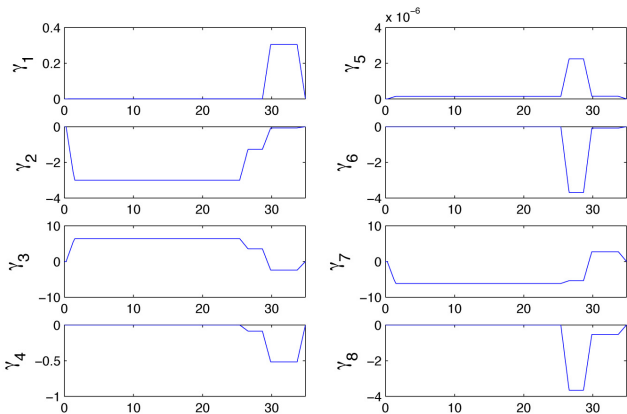


Fig. 3.  $STP_2^E$  eight dimensional thrust strategy for the energy efficient motion ending at  $\eta_{F_2} = (5, 4, 1, 0, 0, 0)$ .

only three thrusters ( $\gamma_2, \gamma_3, \gamma_7$ ) are prescribed significant control forces over the duration of the trajectory. Also, the vertical thrusters are hardly used. From these controls, we can see that the vehicle uses  $\gamma_2$  to provide a slight angular displacement and vertical force, while the horizontal translation is achieved using  $\gamma_3$  and  $\gamma_7$ . This evolution only rotates the vehicle slightly so that energy is not wasted counteracting the potential force of the righting moment or doing unnecessary rotations. Comparing the  $STP_2^E$  consumption efficient strategy to our kinematic motion strategy, we first note the large difference in evolution caused by our under-actuated situation. The kinematic strategy must achieve large inclination angles in order to realize the motion. As seen in Fig. 1, this inclination requires a relatively large control by  $\gamma_6$  and  $\gamma_8$  at the beginning and end of the motion. Also, maintaining this inclination would require significant control if the kinematic motion accounted for potential forces. Without these forces, the energy consumption for our 47 second kinematic motion displayed in Fig. 1 is 247.61Ah. Even though potential forces are omitted, the consumption is one and a half times greater than the  $STP_2^E$  strategy. This additional consumption is related to the time and unique evolution of the motion.

When dealing with energy consumption along a trajectory, we must consider the duration of the motion. Obviously, there will be diminishing returns if the vehicle moves too slow. Also, since we are minimizing consumption, the evolution of a motion will be unique for different time constraints. In Chyba et al. (2008a), the authors present control strategies with duration parameterized by different multiples ( $c_T$ ) of the optimal time (17.43s). The evolution of our kinematic motion nearly resembles that of the evolution of the  $STP_2^E$  consumption efficient trajectory with duration  $c_T = 1.5$ . The consumption for this  $STP_2^E$  strategy is approximately 230Ah, which is close to the consumption of our kinematic motion. Since the kinematic motions depend on the reparameterization  $\tau(t)$ , it is of interest to examine different durations of kinematic motions if energy consumption plays an important role in the application.

## 6. CONCLUSION

As constructed, our geometrically computed kinematic motion ending at  $\eta_{F_2}$  is not yet ready for implementation. Although, with slight modifications, especially in the control of pitch and roll, this strategy could be implemented onto a test-bed AUV. Applying the computed control for pitch and roll throughout the trajectory in an *ad hoc* manner to compensate for the righting moment would be a good first experiment. This is an area of ongoing research and the implementation of kinematic motions similar to those studied in this paper is planned for upcoming testing. Changing the parameterization  $\tau(t)$ , we can construct a more time or energy efficient motion. The specifics of this are currently under investigation.

## REFERENCES

- Francesco Bullo and Andrew D. Lewis. *Geometric Control of Mechanical Systems*. Springer, 2005.
- Francesco Bullo and Kevin Lynch. Kinematic controllability for decoupled trajectory planning in underactuated mechanical systems. *IEEE Transactions. Robotics and Automation*, 17(4):402–412, 2001.
- C. Catone, M. Chyba, R.N. Smith, and G.R. Wilkens. A geometrical approach to the motion planning problem for a submerged rigid body. Unpublished, submitted to *International Journal of Control*, Feb., 2008.
- M. Chyba, T. Haberkorn, R.N. Smith, and G.R. Wilkens. A geometrical analysis of trajectory design for underwater vehicles. Unpublished, submitted to *Discrete and Continuous Dynamical Systems-B*, Oct., 2007.
- M. Chyba, T. Haberkorn, S. Singh, R.N. Smith, and S.K. Choi. Increasing underwater vehicle autonomy by reducing energy consumption. Unpublished, submitted to the *Journal of Ocean Engineering: Special Edition on AUVs*, Jan., 2008a.
- M. Chyba, T. Haberkorn, R.N. Smith, and S.K. Choi. Design and implementation of time efficient trajectories for an underwater vehicle. *Journal of Ocean Engineering*, 35/1:63–76, 2008b.
- M. Chyba, T. Haberkorn, R.N. Smith, and S.K. Choi. Autonomous underwater vehicles: Development and implementation of time and energy efficient trajectories. *Ship Technology Research*, 2008c.